Supplement of Atmos. Chem. Phys., 25, 8907–8927, 2025
https://doi.org/10.5194/acp-25-8907-2025-supplement

Atmospheric Chemistry and Physics
Open Access
EGU

Supplement of

Ozone (O_3) observations in Saxony, Germany, for 1997–2020: trends, modelling and implications for O_3 control

Yaru Wang et al.

Correspondence to: Hartmut Herrmann (herrmann@tropos.de)

Supplement of

Ozone (O_3) observations in Saxony, Germany for 1997 - 2020: Trends, modelling and implications for O_3 control

Yaru Wang[1], Dominik van Pinxteren[1], Andreas Tilgner[1], Erik Hans Hoffmann[1], Max Hell[1], Susanne Bastian[2], Hartmut Herrmann[1*]

[1]Atmospheric Chemistry Department (ACD), Leibniz Institute for Tropospheric Research (TROPOS), Permoserstr. 15, Leipzig, 04318, Germany

[2]Saxon State Office for the Environment, Agriculture, and Geology (LfULG), Pillnitzer Platz 3, Dresden Pillnitz, 01326, Germany

Correspondence to: Hartmut Herrmann (herrmann@tropos.de)

Table S1. Data availability and proportion of missing data of hourly concentrations of ozone in the Saxony air quality measurement network used in the project.

Station	Station type	Begin time	End time	Years	Missing values / %
DD-Nord	Traffic	01.01.1997 00:00	31.12.2020 23:00	24	3.2
Annaberg	Urban	02.01.1997 00:00	31.12.2020 23:00	24	2.3
Bautzen	Urban	01.01.2005 00:00	31.12.2020 23:00	16	0.9
DD-Winkelmannstr.	Urban	19.06.2008 23:00	31.12.2020 23:00	12.5	1.1
L-Thekla	Urban	02.04.2004 00:00	29.04.2020 18:00	16.1	1.6
L-West	Urban	01.01.2000 00:00	31.12.2020 23:00	21	1.8
Plauen-DWD	Urban	20.11.2003 13:00	14.07.2020 08:00	16.7	2.5
Zittau-Ost	Urban	10.01.1997 12:00	31.12.2020 23:00	24	2.3
Collmberg	Rural	30.09.1998 11:00	31.12.2020 23:00	22.3	2.1
Niesky	Rural	05.05.2003 15:00	31.12.2020 23:00	17.7	1.4
Radebeul-Wahnsd.	Rural	01.01.1974 00:00	31.12.2020 23:00	47	3.3
Schkeuditz	Rural	06.06.2003 13:00	31.12.2020 23:00	17.6	1
Carlsfeld	Mountain	01.01.1997 00:00	31.12.2020 23:00	24	2.3
Fichtelberg	Mountain	01.01.1997 00:00	31.12.2020 23:00	24	4.7
Schwartenberg	Mountain	11.02.1998 14:00	31.12.2020 23:00	22.9	2.1
Zinnwald	Mountain	02.01.1997 09:00	31.12.2020 23:00	24	2

Table S2: Availability of further measurement parameters (O_3, NO, NO_2, NO_x, temperature (T), global radiation (GR), relative humidity (RH), wind direction (WD), wind speed (WS), and air pressure) per station.

Station	Station type	O_3	NO	NO_2	NO_x	T	GR	RH	WD	WS	Air pressure
DD-Nord	Traffic	x	x	x	x	x	x	x	x	x	x
Annaberg	Urban	x	x	x	x	x	x	x	x	x	x
Bautzen	Urban	x	x	x	x	x	x	x	x	x	x
DD-Winkelmannstr.	Urban	x	x	x	x	x	x	x	x	x	x
L-Thekla	Urban	x				x	x	x	x	x	x
L-West	Urban	x	x	x	x	x	x	x	x	x	x
Plauen-DWD	Urban	x				x	x	x	x	x	x
Zittau-Ost	Urban	x	x	x	x	x	x	x	x	x	x
Collmberg	Rural	x	x	x	x	x	x	x	x	x	x
Niesky	Rural	x	x	x	x	x	x	x	x	x	x
Radebeul-Wahnsd.	Rural	x	x	x	x	x	x	x	x	x	x
Schkeuditz	Rural	x	x	x	x	x	x	x	x	x	x
Carlsfeld	Mountain	x				x	x	x	x	x	x
Fichtelberg	Mountain	x				x	x	x	x	x	x
Schwartenberg	Mountain	x	x	x	x	x	x	x	x	x	x

Zinnwald	Mountain	x	x	x	x	x	x	x	x	x	x

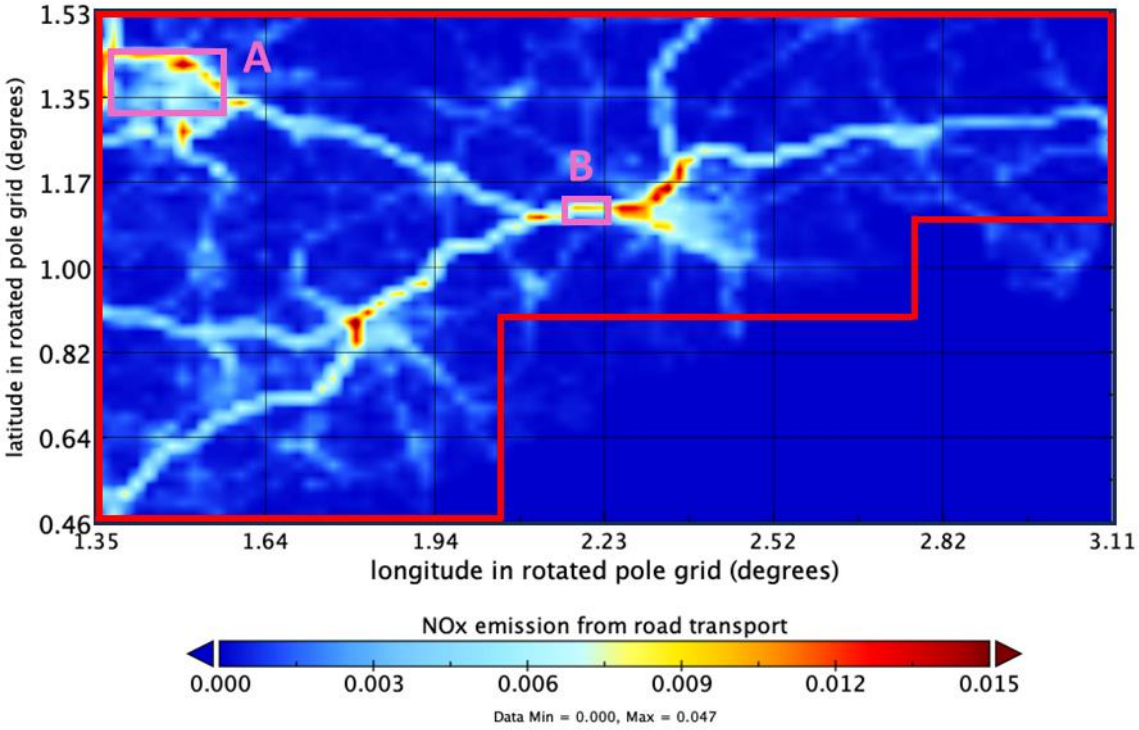

Figure S1: The NO_x emission (in kg m^{-2}) from road transport in the entire Saxony state region in 2019. A continuous red frame indicates the entire simulated Saxony area. Two specific rectangles in rose pink, A and B, represent the representative urban area (city of Leipzig) (0.13° × 0.20°) and traffic-dominated area (highway close to Dresden) (0.07° × 0.10°) used for the simulation, respectively. The covered region indicated with the continuous red frame in Fig. S1 corresponds to the Saxony area in Fig. 1. To convert geographic coordinates to rotated pole coordinates in the figure, the position of the rotated pole (170°W, 40°N) is first defined. The package *pyproj* in *Python* (Python Software Foundation, 2021) is then used to set up the coordinate systems. A transformer is created to convert coordinates from the geographic system (WGS84) to the rotated grid. Once the geographic coordinates are provided, they are automatically transformed into rotated pole latitude and longitude.

Table S3. The annual emission data in 2019 for the entire Saxony region in summer and winter simulation scenarios. Each species is given by its SMILES string, and its IUPAC name generated using the PubChemPy package in Python (https://pubchempy.readthedocs.io/en/latest/), along with the corresponding chemical structure. It is noted that for some compounds, IUPAC names could not be retrieved from the PubChem database by the tool and they are therefore left blank.

See attached Excel file named *Table S3_ The annual emission data in 2019 for the entire Saxony region.*

Table S4. Modelling configuration and settings for summer and winter scenarios.

Model setting	Unit	Summer	Winter	Reference
Initial time		00:00 CET, 14 July, 2019	00:00 CET, 14 January, 2019	
Meteorological conditions				
Temperature	°C	15	4	Measured
Pressure	hPa	1000	1000	Measured
Relative humidity	%	70	70	Measured
Ratio of Solar radiation*		0.7	0.4	Measured
Dry deposition velocity				

NO_2	cm s^{-1}	0.3	3	Rondón et al. (1993)
N_2O_5	cm s^{-1}	100	2	Hoffmann et al. (2019)
O_3	cm s^{-1}	0.8	0.08	Clifton et al. (2020)
NO	cm s^{-1}	0.05	0.05	Zhu et al. (2020)
HNO_3	cm s^{-1}	3.5	3.5	Zhu et al. (2020)
H_2O_2	cm s^{-1}	1	1	Zhu et al. (2020)
CO	cm s^{-1}	0.1	0.1	Zhu et al. (2020)
HCl	cm s^{-1}	1	1	Zhu et al. (2020)
NH_3	cm s^{-1}	1	1	Zhu et al. (2020)
SO_2	cm s^{-1}	1	1	Zhu et al. (2020)
H_2SO_4	cm s^{-1}	2	2	Zhu et al. (2020)
HCHO	cm s^{-1}	1	1	Zhu et al. (2020)
CH_3OH	cm s^{-1}	1	1	Zhu et al. (2020)
CH_3CH_2OH	cm s^{-1}	0.5	0.5	Zhu et al. (2020)
PANs	cm s^{-1}	0.7	0.7	Wu et al. (2012)
CHClO	cm s^{-1}	0.2	0.2	Hoffmann et al. (2019)
CHBrO	cm s^{-1}	0.2	0.2	Hoffmann et al. (2019)
Boundary layer heights (BLHs)				
Daytime BLHs	m	500	2000	
Nighttime BLHs	m	250	1000	
Measured Chemical data				
O_3	ppb	31.7	21.6	Measured
NO_2	ppb	3.4	7.0	Measured
SO_2	ppb	1.1	1.9	UBA website
CO	ppb	153.4	153.4	Zellweger et al. (2009)
CH_4	ppb	1700	1700	Herrmann et al. (2000)
HONO	ppb	0.5	0.5	Stieger et al. (2018)
PAN	ppb	0.5	0.5	Pandey Deolal et al. (2014)

* Ratio of solar radiation, defined as the mean value between 10:00 and 14:00 (CET) divided by the maximum clear sky radiation value during the same period.

Table S5. Dominant initial gas-phase concentrations applied in the final 24-hour simulations for summer and winter scenarios. Each species is given by its SMILES string, and its IUPAC name generated using the PubChemPy package in Python (https://pubchempy.readthedocs.io/en/latest/), along with the corresponding chemical structure. It is noted that for some compounds, IUPAC names could not be retrieved from the PubChem database by the tool and they are therefore left blank.

See attached Excel file named *Table S5_Dominant initial gas-phase concentrations.*

Table S6. Changing the emission multiplier for NO_x and TNMVOC in the simulations. Two or three batches were conducted for each season, considering each combination, with each batch comprising 400 model runs. The total number of simulations is 800 for summer and 1200 for winter.

Batch 1 (Summer/Winter)			Batch 2 (Summer/Winter)			Batch 3 (Winter)		
Number	Emission factor		Number	Emission factor		Number	Emission factor	
	NO_x	TNMVOC		NO_x	TNMVOC		NO_x	TNMVOC
1	0.001	0.001	**1**	1.5	1.5	**1**	1.5	13
2	0.005	0.005	**2**	2	2	**2**	2	14
3	0.01	0.01	**3**	2.5	2.5	**3**	2.5	16
4	0.05	0.05	**4**	3	3	**4**	3	17
5	0.1	0.1	**5**	3.5	3.5	**5**	3.5	18

6	0.5	0.5	**6**	4	4	**6**	4	19
7	1	1	**7**	4.5	4.5	**7**	4.5	21
8	5	5	**8**	5.5	5.5	**8**	5.5	22
9	10	10	**9**	6	6	**9**	6	23
10	15	15	**10**	6.5	6.5	**10**	6.5	24
11	20	20	**11**	7	7	**11**	7	26
12	25	25	**12**	7.5	7.5	**12**	7.5	27
13	30	30	**13**	8	8	**13**	8	28
14	35	35	**14**	8.5	8.5	**14**	8.5	29
15	40	40	**15**	9	9	**15**	9	30
16	45	45	**16**	9.5	9.5	**16**	9.5	31
17	50	50	**17**	10.5	10.5	**17**	10.5	32
18	60	60	**18**	11	11	**18**	11	33
19	70	70	**19**	11.5	11.5	**19**	11.5	34
20	80	80	**20**	12	12	**20**	12	35
Total simulation number	**400**		**400**			**400**		

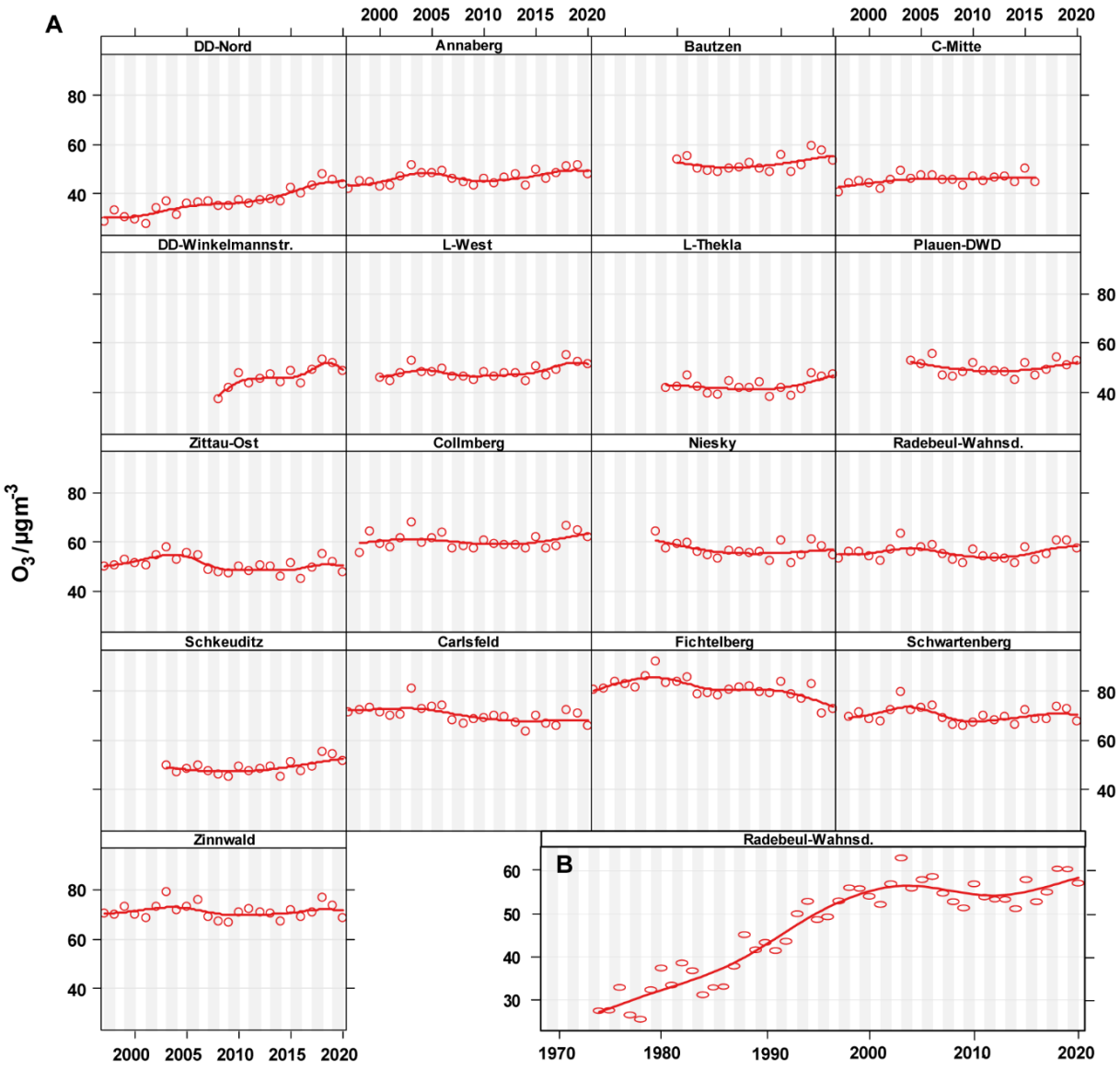

Figure S2: Smooth trends in annual means of O_3 for A) all stations from 1997 (or later) to 2020 and B) Radebeul-Wahnsdorf from 1974 - 2020.

Table S7. Trends of the mean ozone concentration at the stations of the Saxony air quality monitoring network for three different time periods. Statistically non-significant values with p > 0.05 are put in brackets. * means the years begin from 2008.

Station	Station type	All available years		15 years		10 years	
		1997 (or later) until 2020		2006 to 2020		2011 to 2020	
		abs. Trend	rel. Trend	abs. Trend	rel. Trend	abs. Trend	rel. Trend
		µg m^{-3} year^{-1}	% year^{-1}	µg m^{-3} year^{-1}	% year^{-1}	µg m^{-3} year^{-1}	% year^{-1}
DD-Nord	Traffic	0.65	2.30	0.75	2.27	1.19	3.50
Annaberg	Urban	0.17	0.38	0.28	0.63	0.51	1.14
Bautzen	Urban	0.24	0.47	0.35	0.72	0.59	1.19
DD-Winkelmannstr.	Urban	0.65	1.57	0.65*	1.57*	0.74	1.75
L-West	Urban	0.19	0.42	0.38	0.83	0.64	1.42
L-Thekla	Urban	(0.15)	(0.37)	(0.13)	(0.32)	0.51	1.28
Plauen-DWD	Urban	(-0.09)	(-0.17)	(0.09)	(0.20)	(0.41)	(0.85)
Zittau-Ost	Urban	-0.14	-0.27	(0.03)	(0.06)	(0.24)	(0.51)
Collmberg	Rural	(-0.03)	(-0.05)	0.26	0.45	0.53	0.92
Niesky	Rural	(-0.13)	(-0.23)	(0.05)	(0.10)	(0.15)	(0.28)
Radebeul-Wahnsd.	Rural	(0.05)	(0.09)	0.27	0.52	0.71	1.38
Schkeuditz	Rural	0.25	0.53	0.43	0.93	0.68	1.49
Carlsfeld	Mountain	-0.26	-0.35	(-0.12)	(-0.17)	(0.00)	(-0.01)
Fichtelberg	Mountain	-0.31	-0.37	-0.37	-0.45	-0.79	-0.95
Schwartenberg	Mountain	(-0.05)	(-0.06)	(0.15)	(0.22)	(0.26)	(0.37)
Zinnwald	Mountain	(-0.02)	(-0.03)	(0.15)	(0.22)	(0.14)	(0.20)

Table S8. Trends for all available years since 1997, 15 years from 2006 to 2020 and 10 years from 2011 to 2020 of NO_x (A), NO (B), NO_2 (C), and O_x (D). Statistically non-significant values with p > 0.05 are put in brackets. * means the years begin from 2008.

(A)

NO_x		All available years		15 years		10 years	
		1997 or later - 2020		2006 - 2020		2011 - 2020	
Station	Station type	abs. Trend	rel. Trend	abs. Trend	rel. Trend	abs. Trend	rel. Trend
		µg m^{-3} year^{-1}	% year^{-1}	µg m^{-3} year^{-1}	% year^{-1}	µg m^{-3} year^{-1}	% year^{-1}
DD-Nord	Traffic	-2.96	-2.57	-3.32	-3.54	-3.83	-4.77
Annaberg	Urban	-1.66	-2.46	-1.60	-2.98	-1.56	-3.42
Bautzen	Urban	-1.13	-3.09	-1.13	-3.19	-1.32	-4.27
DD-Winkelmannstr.	Urban	-0.90	-2.75	-0.90*	-2.75*	-0.90	-3.03
L-West	Urban	-0.57	-1.88	-0.58	-2.17	-0.75	-3.06
L-Thekla	Urban						
Plauen-DWD	Urban						
Zittau-Ost	Urban	-0.30	-1.35	-0.22	-1.18	-0.50	-2.59
Collmberg	Rural	-0.31	-1.89	-0.36	-2.55	-0.37	-2.99
Niesky	Rural	-0.24	-2.04	-0.24	-2.04	-0.15	-1.41
Radebeul-Wahnsd.	Rural	-0.44	-1.77	-0.48	-2.26	-0.56	-2.97
Schkeuditz	Rural						
Carlsfeld	Mountain						
Fichtelberg	Mountain						

Schwartenberg	Mountain	-0.36	-2.13	-0.40	-2.91	-0.30	-2.71
Zinnwald	Mountain	-0.40	-2.22	-0.46	-3.27	-0.32	-2.92

(B)

NO		**All available years**		**15 years**		**10 years**	
		1997 or later - 2020		**2006 - 2020**		**2011 - 2020**	
Station	**Station type**	**abs. Trend**	**rel. Trend**	**abs. Trend**	**rel. Trend**	**abs. Trend**	**rel. Trend**
		µg m^{-3} year^{-1}	**% year^{-1}**	**µg m^{-3} year^{-1}**	**% year^{-1}**	**µg m^{-3} year^{-1}**	**% year^{-1}**
DD-Nord	Traffic	-1.22	-2.93	-1.27	-4.02	-1.49	-5.53
Annaberg	Urban	-0.65	-2.78	-0.60	-3.33	-0.70	-4.61
Bautzen	Urban	-0.29	-3.46	-0.29	-3.62	-0.31	-4.59
DD-Winkelmannstr.	Urban	-0.11	-2.09	-0.11*	-2.09*	-0.15	-2.96
L-West	Urban	-0.07	-1.62	-0.05	-1.34	-0.10	-2.74
L-Thekla	Urban						
Plauen-DWD	Urban						
Zittau-Ost	Urban	-0.02	-0.78	-0.01	-0.60	-0.10	-2.98
Collmberg	Rural	-0.01	-0.44	0.00	-0.18	-0.01	-0.48
Niesky	Rural	-0.01	-0.85	-0.01	-0.85	-0.02	-1.26
Radebeul-Wahnsd.	Rural	-0.03	-1.07	-0.02	-0.90	-0.05	-2.04
Schkeuditz	Rural						
Carlsfeld	Mountain						
Fichtelberg	Mountain						
Schwartenberg	Mountain	-0.01	-0.69	-0.01	-1.01	-0.02	-1.53
Zinnwald	Mountain	-0.02	-1.24	-0.01	-0.99	(-0.01)	(-0.43)

(C)

NO_2		**All available years**		**15 years**		**10 years**	
		1997 or later - 2020		**2006 - 2020**		**2011 - 2020**	
Station	**Station type**	**abs. Trend**	**rel. Trend**	**abs. Trend**	**rel. Trend**	**abs. Trend**	**rel. Trend**
		µg m^{-3} year^{-1}	**% year^{-1}**	**µg m^{-3} year^{-1}**	**% year^{-1}**	**µg m^{-3} year^{-1}**	**% year^{-1}**
DD-Nord	Traffic	-1.06	-2.06	-1.40	-3.10	-1.56	-3.99
Annaberg	Urban	-0.65	-2.02	-0.69	-2.61	-0.57	-2.54
Bautzen	Urban	-0.68	-2.82	-0.68	-2.95	-0.78	-3.84
DD-Winkelmannstr.	Urban	-0.63	-2.65	-0.63*	-2.65*	-0.58	-2.71
L-West	Urban	-0.45	-1.91	-0.51	-2.39	-0.57	-3.04
L-Thekla	Urban						

Plauen-DWD	Urban						
Zittau-Ost	Urban	-0.26	-1.50	-0.25	-1.64	-0.32	-2.24
Collmberg	Rural	-0.29	-2.04	-0.35	-2.83	-0.34	-3.33
Niesky	Rural	-0.21	-2.25	-0.21	-2.25	(-0.10)	(-1.20)
Radebeul-Wahnsd.	Rural	-0.39	-1.86	-0.44	-2.48	-0.51	-3.25
Schkeuditz	Rural						
Carlsfeld	Mountain						
Fichtelberg	Mountain						
Schwartenberg	Mountain	-0.33	-2.34	-0.38	-3.28	-0.29	-3.23
Zinnwald	Mountain	-0.36	-2.39	-0.43	-3.77	-0.35	-3.89

(D)

O_x		**All available years**		**15 years**		**10 years**	
		1997 or later - 2020		**2006 - 2020**		**2011 - 2020**	
Station	**Station type**	**abs. Trend**	**rel. Trend**	**abs. Trend**	**rel. Trend**	**abs. Trend**	**rel. Trend**
		µg m^{-3} $year^{-1}$	**% $year^{-1}$**	**µg m^{-3} $year^{-1}$**	**% $year^{-1}$**	**µg m^{-3} $year^{-1}$**	**% $year^{-1}$**
DD-Nord	Traffic	-0.21	-0.52	-0.33	-0.82	-0.26	-0.68
Annaberg	Urban	-0.24	-0.62	-0.23	-0.63	(-0.09)	(-0.25)
Bautzen	Urban	-0.25	-0.67	-0.21	-0.56	(-0.20)	(-0.55)
DD-Winkelmannstr.	Urban	(-0.07)	(-0.22)	(-0.07) *	(-0.22) *	(-0.03)	(-0.07)
L-West	Urban	-0.14	-0.40	(-0.10)	(-0.28)	(-0.07)	(-0.21)
L-Thekla	Urban						
Plauen-DWD	Urban						
Zittau-Ost	Urban	-0.22	-0.63	-0.14	-0.43	(-0.13)	(-0.41)
Collmberg	Rural	-0.16	-0.43	(-0.08)	(-0.24)	-0.02	-0.05
Niesky	Rural	(-0.13)	(-0.40)	(-0.13)	(-0.40)	(-0.04)	(-0.12)
Radebeul-Wahnsd.	Rural	-0.17	-0.45	-0.10	-0.29	-0.03	-0.10
Schkeuditz	Rural						
Carlsfeld	Mountain						
Fichtelberg	Mountain						
Schwartenberg	Mountain	-0.20	-0.46	-0.17	-0.41	(-0.08)	(-0.21)
Zinnwald	Mountain	-0.18	-0.42	-0.17	-0.43	(-0.16)	(-0.41)

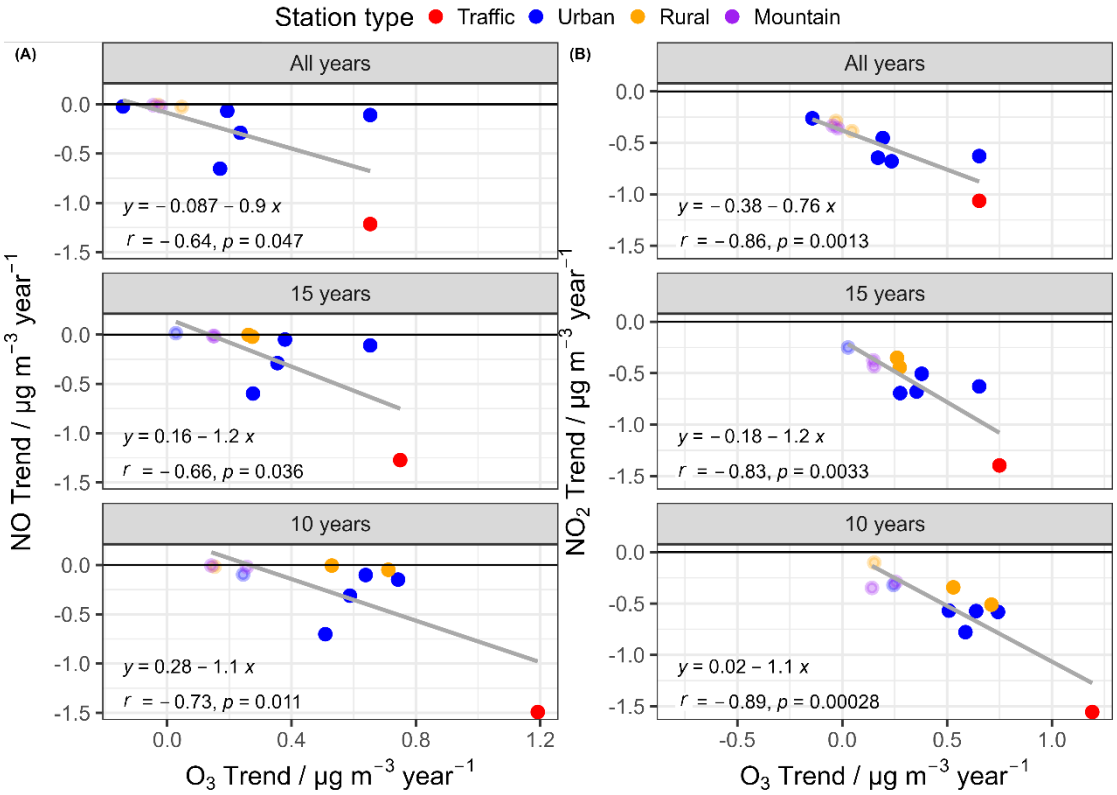

Figure S3: Relationships between O_3 trends and NO, NO_2 trends across all stations for three different time periods (given in rows 1-3). Coloured dots show the values of individual stations, with solid dots for statistically significant O_3 trends and transparent dots otherwise. Also shown are linear fits for O_3 trends and NO, NO_2 trends in different time periods.

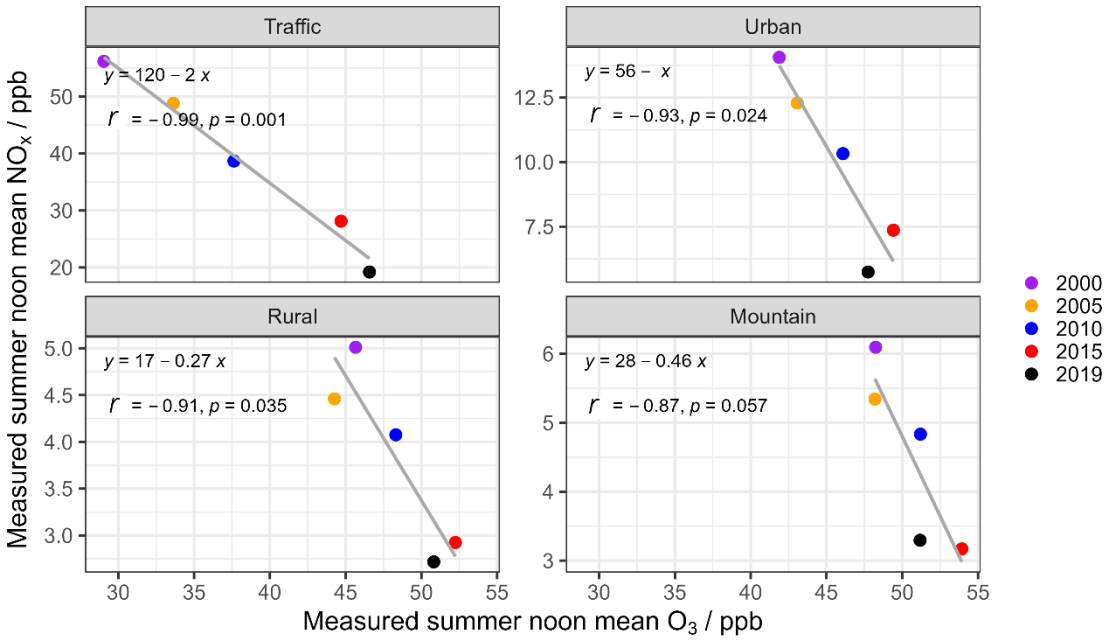

Figure S4: Linear correlations between measured averaged noon (12:00 - 13:00) NO_x and O_3 in ppb of four station types in summer over 5 years (2000, 2005, 2010, 2015 and 2019). For better comparability with mass-based concentrations elsewhere in the manuscript, conversion factors of NO_x (µg m^{-3}) ≈ 1.5 × NO_x (ppb) and O_3 (µg m^{-3}) ≈ 2 × O_3 (ppb) can be used.

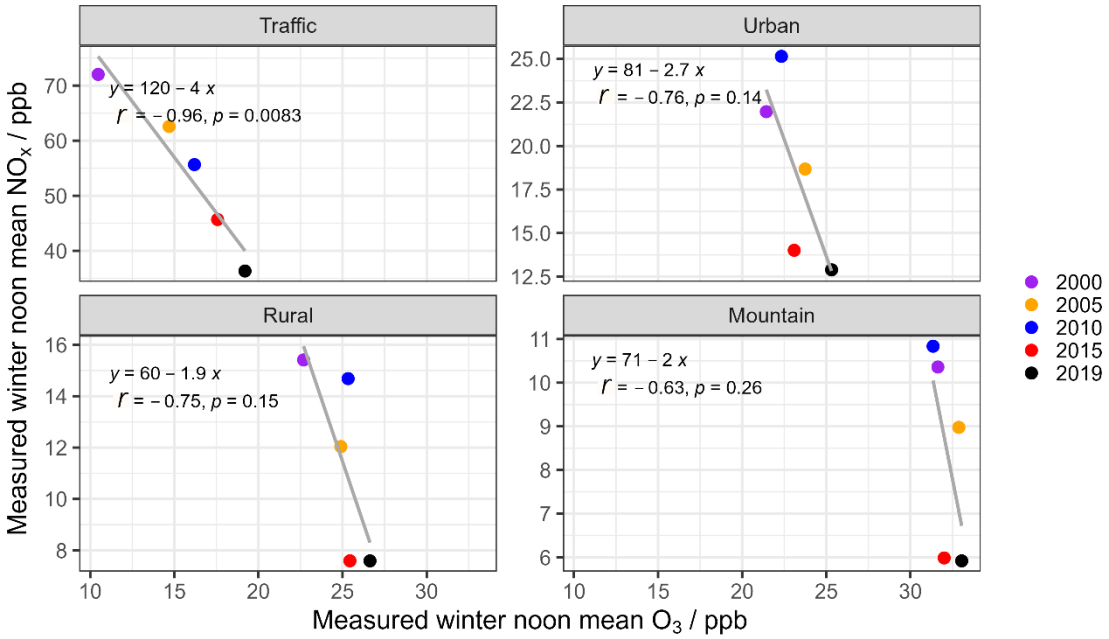

Figure S5: Linear correlations between measured averaged noon (12:00 - 13:00) NO_x and O_3 in ppb of four station types in winter over 5 years (2000, 2005, 2010, 2015 and 2019). For better comparability with mass-based concentrations elsewhere in the manuscript, conversion factors of NO_x (µg m^{-3}) ≈ 1.5 × NO_x (ppb) and O_3 (µg m^{-3}) ≈ 2 × O_3 (ppb) can be used.

Definition of the normalized mean bias factor (NMBF) as a model performance evaluation metric

The hourly average concentrations of NO, O_3, and NO_2 observed (O) across rural background sites in Saxony are calculated in the same way as the modelled hourly averages (M). To evaluate the model performance for each pollutant, the NMBF is used as a statistical metric (Yu et al., 2006; Jaidan et al., 2018), defined as follows:

$$NMBF = \frac{\sum_{i=1}^{n}(M_i - O_i)}{\sum_{i=1}^{n} O_i}$$

where n is the number of hourly mean values for NO, O_3 and NO_2.

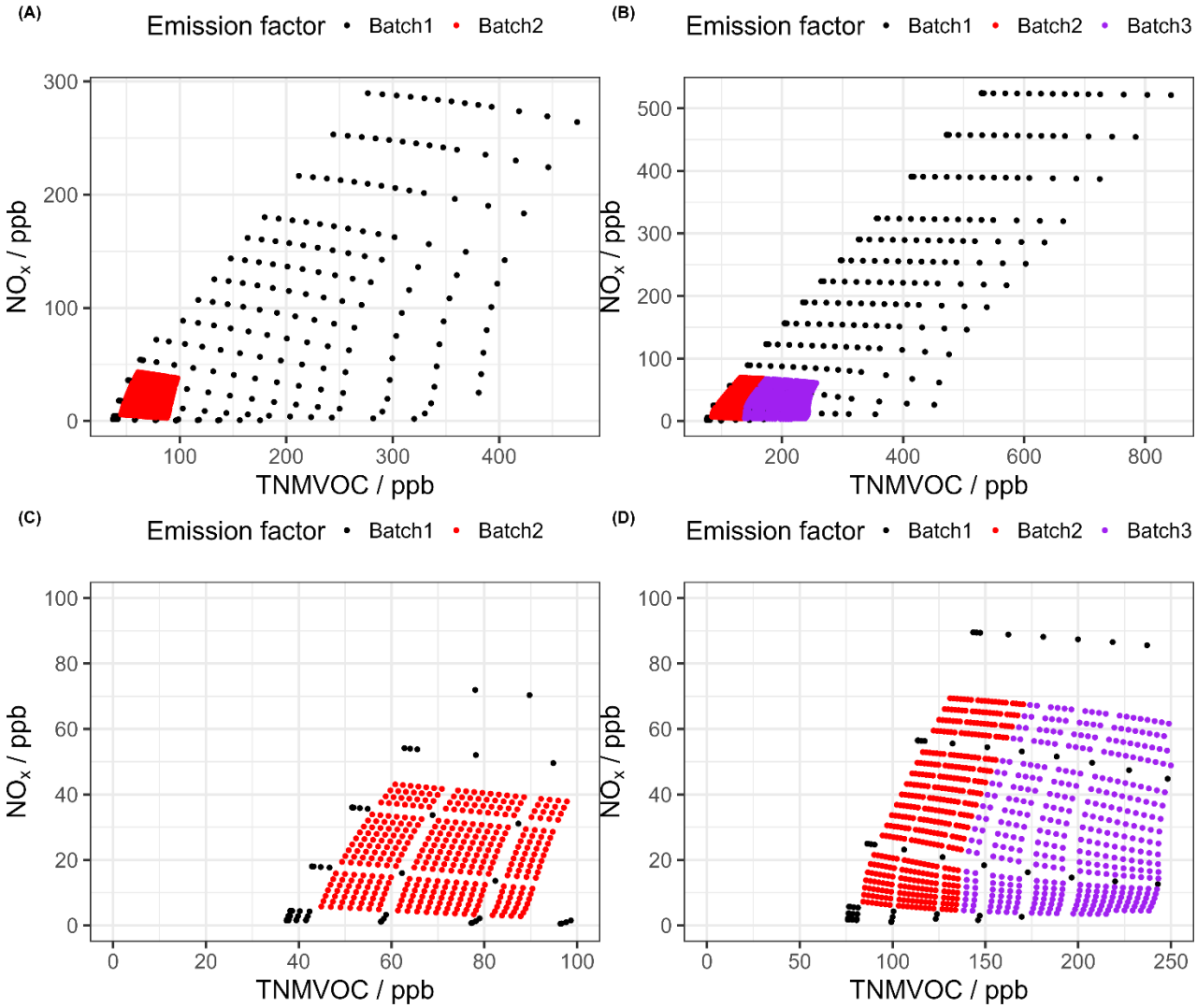

Figure S6: The distribution of resulting TNMVOC and NO_x concentrations (in ppb) based on a total of 800 and 1200 model runs (see Table S6 for details) for summer (A) and winter (B), respectively. Panels C (summer) and D (winter) are subsets of Panels A and B, respectively, and use the same concentration coordinate ranges as Fig. S7. The different colors indicate different batch runs.

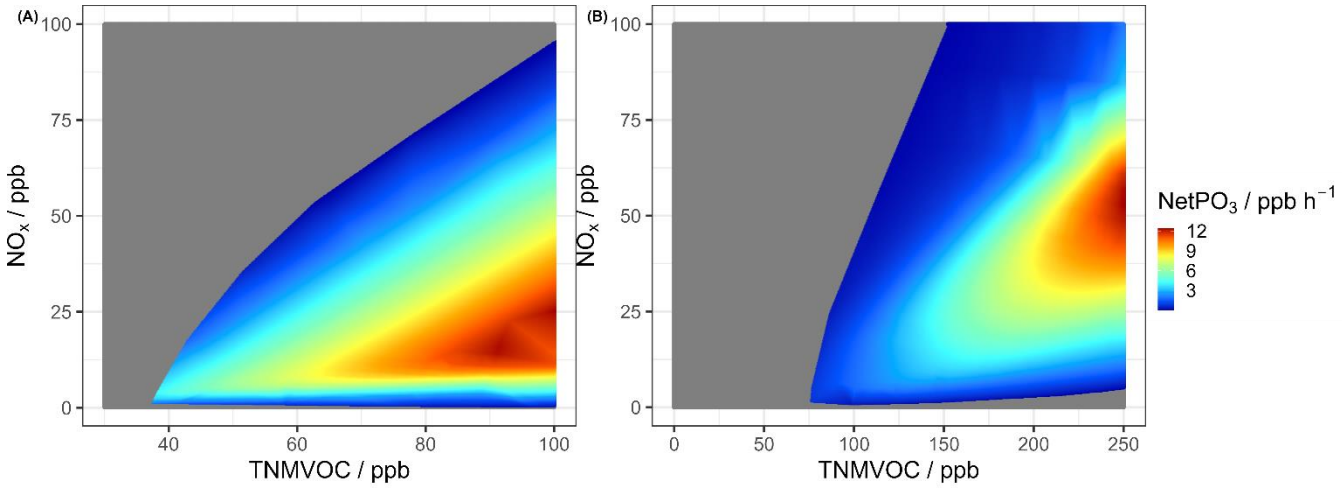

Figure S7: The grid of modelled net O_3 production rate ($NetPO_3$ in ppb h^{-1}) during 12:00 - 13:00 CET as a function of both modelled and emission inventory-derived NO_x and TNMVOC concentrations (in ppb) (see Sect. 2.3) after bivariate linear interpolation. The X-axis and Y-axis in both summer (A) and winter (B) are interpolated using a very fine-resolved 1000 × 1000 grid. $NetPO_3$ is shown using a rainbow color scale.

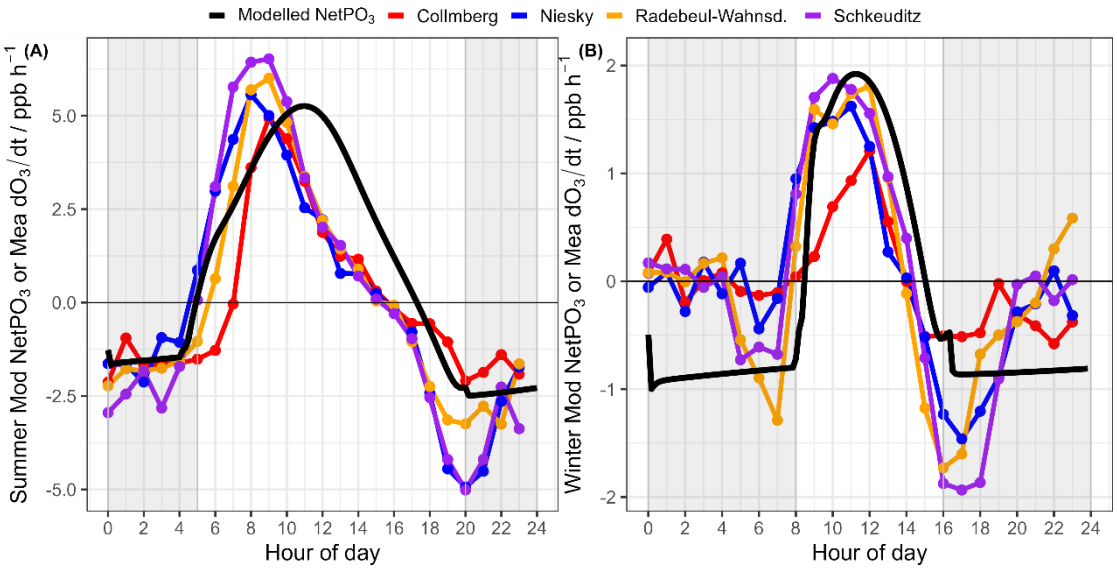

Figure S8: Diurnal profiles of the modelled net O_3 production rate ($NetPO_3$ in ppb h^{-1}) and measured O_3 change rate (dO_3/dt, ppb h^{-1} in Saxony at rural background sites (A and B for summer and winter cases, respectively). Shaded areas indicate night-time, black line indicates the modelled $NetPO_3$ and other coloured lines refer to the observed dO_3/dt at each station. Linear correlation coefficient (r) between modelled and measured rates is larger than 0.8 in both seasons.

Table S9. TNMVOC concentrations for the summer scenario used to include station type data into the isopleth diagram (Fig. 10 A). These are derived from comparing measured and modelled NO_x, as well as measured dO_3/dt and modelled $NetPO_3$ values.

				Measured		Modelled		
Year	**Period**	**Hour**	**Station type**	**NO_x**	**dO_3/dt**	**NO_x**	**$NetPO_3$**	**TNMVOC**
				ppb	ppb h^{-1}	ppb	ppb h^{-1}	ppb
2000	Summer	6 - 12	Traffic	65.22	2.74	65.27	2.74	91.87
2000	Summer	6 - 12	Urban	19.07	4.13	19.02	4.13	54.06
2000	Summer	6 - 12	Rural	8.49	2.89			
2000	Summer	6 - 12	Mountain	7.15	1.20			
2005	Summer	6 - 12	Traffic	59.17	3.69	59.16	3.69	90.70
2005	Summer	6 - 12	Urban	18.27	4.27	18.22	4.27	53.80
2005	Summer	6 - 12	Rural	7.06	3.45			
2005	Summer	6 - 12	Mountain	6.22	1.16			
2010	Summer	6 - 12	Traffic	45.62	3.87	45.65	3.87	78.79
2010	Summer	6 - 12	Urban	15.08	4.63	15.12	4.63	52.05
2010	Summer	6 - 12	Rural	5.94	3.42			
2010	Summer	6 - 12	Mountain	5.53	1.18			
2015	Summer	6 - 12	Traffic	34.27	4.32	34.23	4.32	69.81
2015	Summer	6 - 12	Urban	11.48	4.75	11.51	4.75	48.60
2015	Summer	6 - 12	Rural	4.96	3.73			
2015	Summer	6 - 12	Mountain	3.94	1.30			
2019	Summer	6 - 12	Traffic	23.87	4.55	23.82	4.55	60.64
2019	Summer	6 - 12	Urban	9.59	4.88	9.61	4.87	46.91
2019	Summer	6 - 12	Rural	4.54	3.89			
2019	Summer	6 - 12	Mountain	3.67	1.64			

Table S10. TNMVOC concentrations for the winter scenario used to include station type data into the isopleth diagram (Fig. 10 B). These are derived from comparing measured and modelled NO_x, as well as measured dO_3/dt and modelled $NetPO_3$ values.

				Measured		Modelled		
Year	**Period**	**Hour**	**Station type**	**NO_x**	**dO_3/dt**	**NO_x**	**$NetPO_3$**	**TNMVOC**
				ppb	ppb h^{-1}	ppb	ppb h^{-1}	ppb
2000	Winter	8 - 12	Traffic	80.56	0.78	80.58	0.78	178.88
2000	Winter	8 - 12	Urban	31.48	1.45	31.43	1.46	108.46
2000	Winter	8 - 12	Rural	16.38	0.97			
2000	Winter	8 - 12	Mountain	10.46	0.69			
2005	Winter	8 - 12	Traffic	68.96	0.85	68.97	0.85	164.34
2005	Winter	8 - 12	Urban	23.16	1.22	23.12	1.22	92.69
2005	Winter	8 - 12	Rural	12.87	0.99			
2005	Winter	8 - 12	Mountain	8.42	0.44			
2010	Winter	8 - 12	Traffic	63.24	0.98	63.26	0.98	157.86
2010	Winter	8 - 12	Urban	29.75	1.32	29.73	1.32	104.25
2010	Winter	8 - 12	Rural	15.34	1.30			
2010	Winter	8 - 12	Mountain	10.08	0.68			
2015	Winter	8 - 12	Traffic	55.01	1.42	55.06	1.42	150.50
2015	Winter	8 - 12	Urban	20.24	1.61	20.22	1.61	93.22
2015	Winter	8 - 12	Rural	9.11	1.17			
2015	Winter	8 - 12	Mountain	5.97	0.48			
2019	Winter	8 - 12	Traffic	43.47	1.59	43.44	1.59	131.06
2019	Winter	8 - 12	Urban	18.16	1.65	18.12	1.65	90.94
2019	Winter	8 - 12	Rural	8.85	1.17			
2019	Winter	8 - 12	Mountain	5.67	0.35			

Table S11. The species list of NMVOCs measured by online thermodesorption gas chromatography with flame ionization detection in Borna, south of Leipzig, Germany.

Number	Compounds
1	1-Butene
2	1-Hexene
3	1-Pentene
4	1,2,3-Trimethylbenzene
5	1,2,4-Trimethylbenzene
6	1,3-Butadiene
7	1,3,5-Trimethylbenzene
8	2-Methylheptane
9	2-Methylhexane
10	2-Methylpentane
11	2,2-Dimethylbutane
12	2,2,4-Trimethylpentane
13	2,3-Dimethylbutane
14	2,3-Dimethylpentane
15	2,3,4-Trimethylpentane
16	2,4-Dimethylpentane
17	3-Methylheptane
18	3-Methylhexane
19	3-Methylpentane
20	a-Pinene
21	Acetylene

22	b-Pinene
23	Benzene
24	cis-2-Butene
25	cis-2-Pentene
26	Cyclohexane
27	Cyclopentane
28	Ethane
29	Ethene
30	Ethylbenzene
31	i-Butane
32	i-Butene
33	i-Pentane
34	i-Propylbenzene
35	Isoprene
36	Limonene
37	m-Diethylbenzene
38	m-Ethyltoluene
39	m,p-Xylene
40	Methylcyclohexane
41	Methylcyclopentane
42	n-Butane
43	n-Decane
44	n-Dodecane
45	n-Heptane
46	n-Hexane
47	n-Nonane
48	n-Octane
49	n-Pentane
50	n-Propylbenzene
51	n-Undecane
52	o-Ethyltoluene
53	o-Xylene
54	p-Diethylbenzene
55	p-Ethyltoluene
56	Propane
57	Propene
58	Styrene
59	Toluene
60	trans-2-Butene
61	trans-2-Pentene
62	1-Hexene
63	2,2-Dimethylbutane
64	3-Methylpentane
65	Butadiene
66	n-Hexane

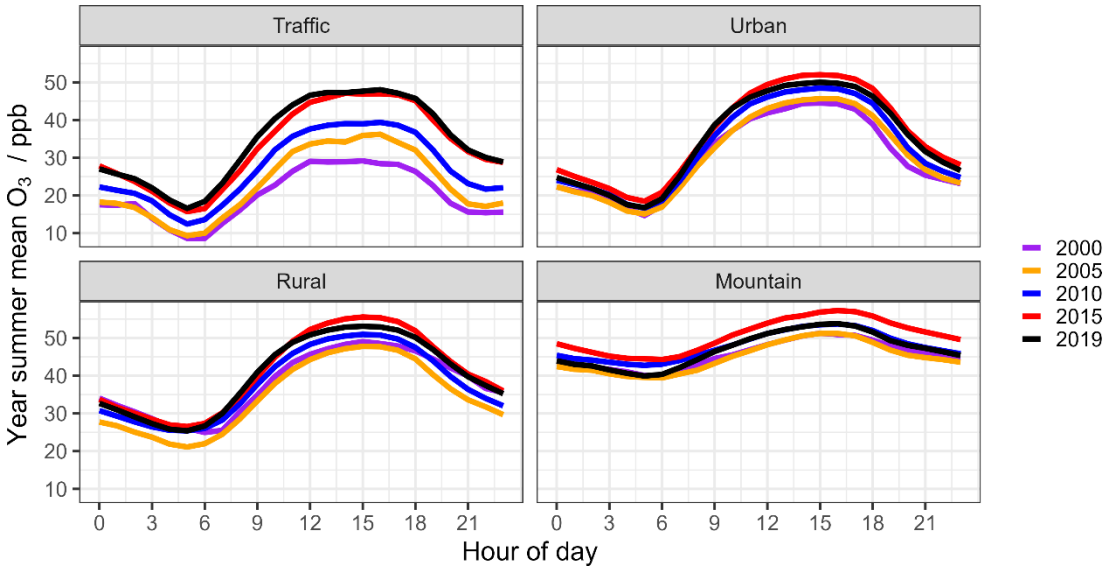

Figure S9: Diurnal profiles of hourly averaged measured O_3 in summer over five years (2000, 2005, 2010, 2015, and 2019) across four station types.

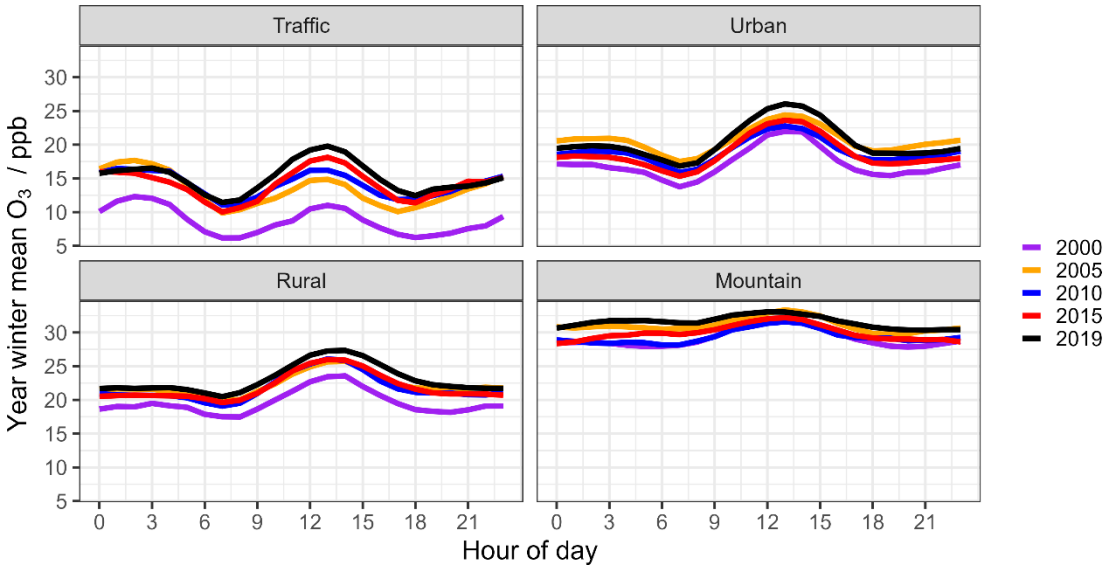

Figure S10: Diurnal profiles of hourly averaged measured O_3 in winter over five years (2000, 2005, 2010, 2015, and 2019) across four station types.

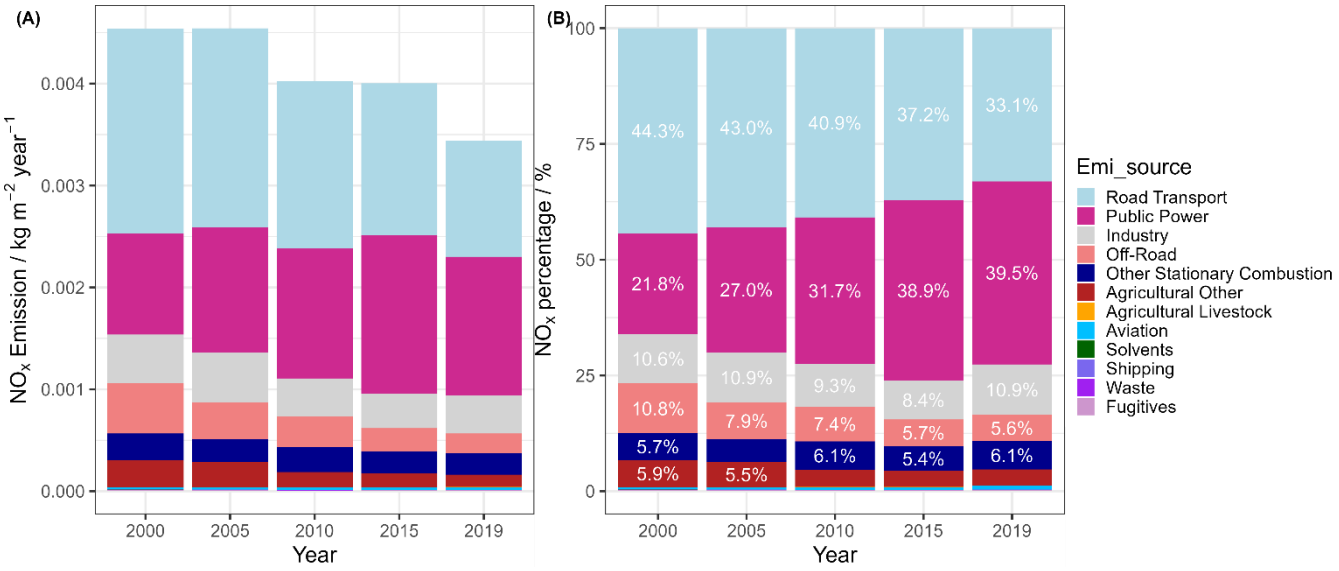

Figure S11: Anthropogenic emissions of NO_x in Saxony for five years between 2000 and 2019. Emission data were obtained by averaging values for each year across the approximated area of the entire state of Saxony (see Fig. S1). Details of the emission categories and corresponding emission sectors can be found in Table S13.

125

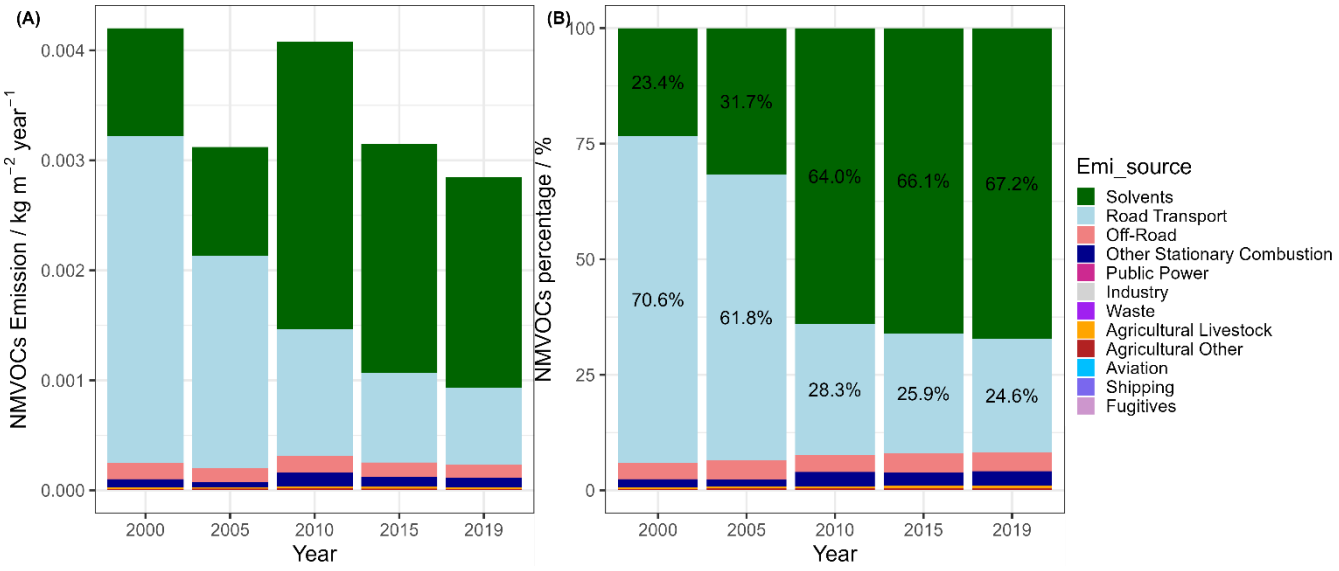

Figure S12: Anthropogenic emissions of NMVOCs in traffic area for five years between 2000 and 2019. Emission data were obtained by averaging values for each year from the selected traffic-dominated area (see Fig. S1). Details of the emission categories and corresponding emission sectors can be found in Table S13.

130

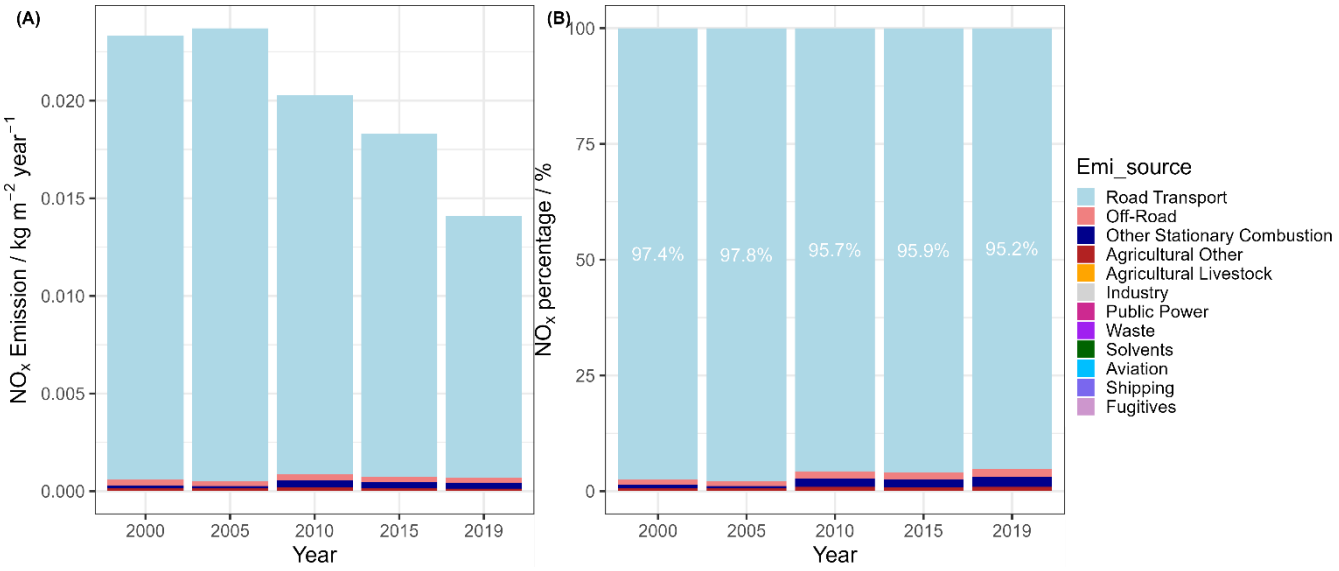

Figure S13: Anthropogenic emission of NO_x in traffic area for five years between 2000 and 2019. Emission data were obtained by averaging values for each year from the selected traffic-dominated area (see Fig. S1). Details of the emission categories and corresponding emission sectors can be found in Table S13.

135

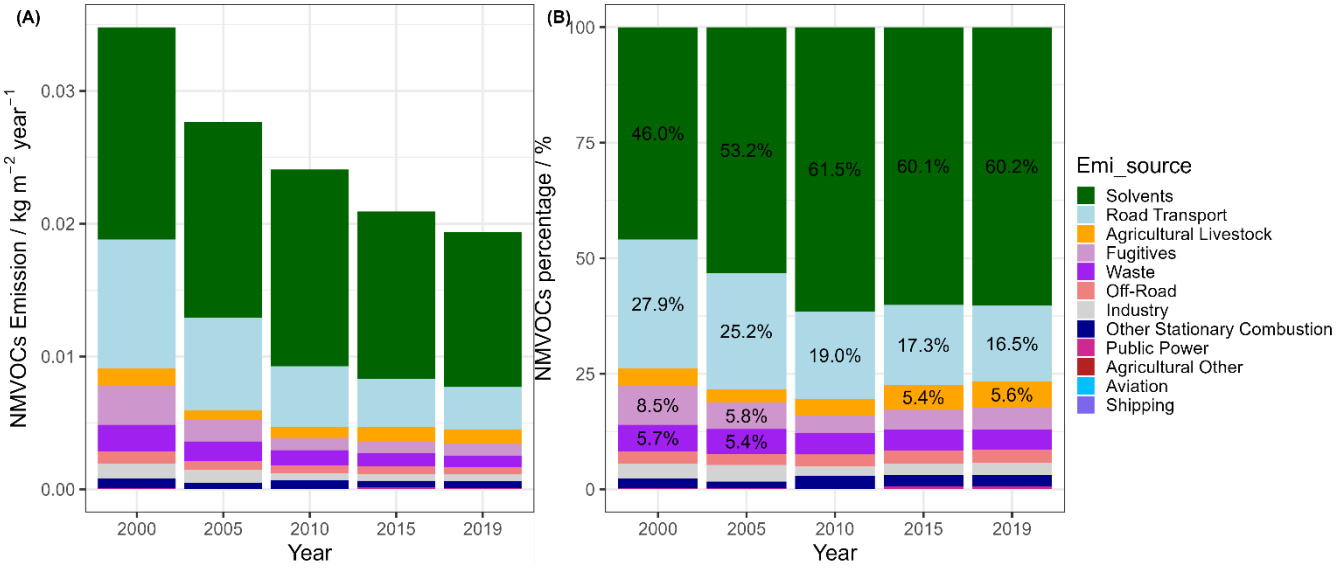

Figure S14: Anthropogenic emission of NMVOCs in urban area for five years between 2000 and 2019. Emission data were obtained by averaging values for each year from the selected urban area (city of Leipzig) (see Fig. S1). Details of the emission categories and corresponding emission sectors can be found in Table S13.

140

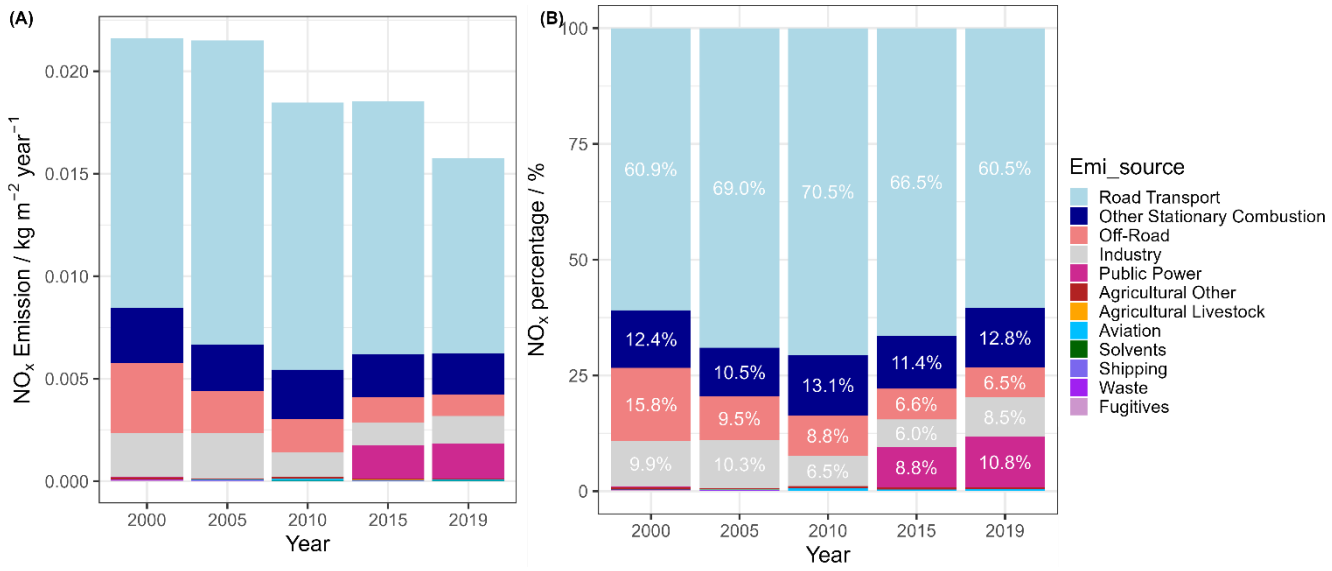

Figure S15: Anthropogenic emission NO_x in urban area for five years between 2000 and 2019. Emission data were obtained by averaging values for each year from the selected urban area (city of Leipzig) (see Fig. S1). Details of the emission categories and corresponding emission sectors can be found in Table S13.

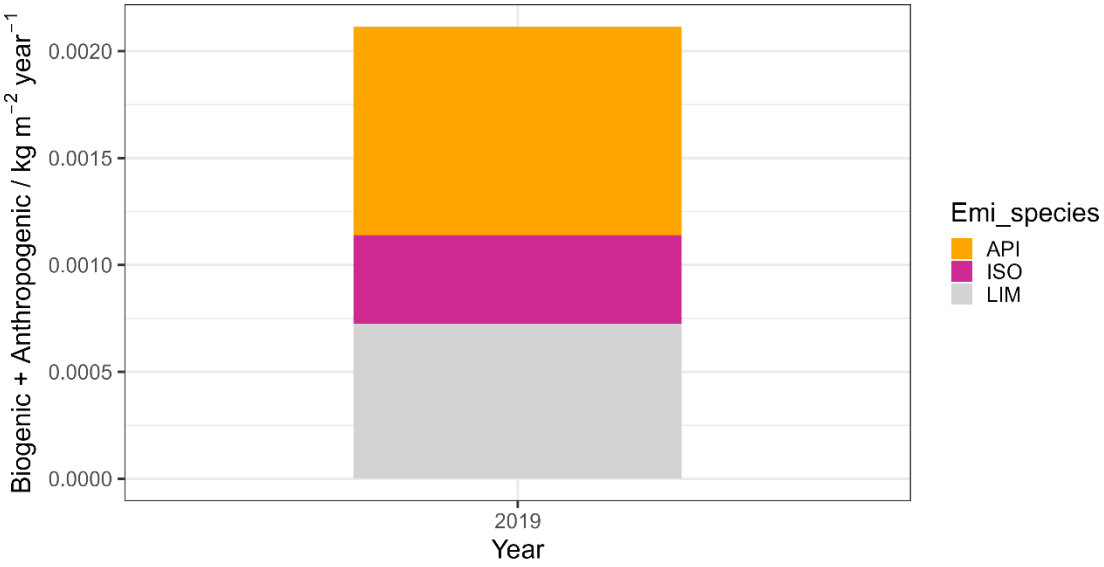

Figure S16: Biogenic emissions of isoprene (ISO) and alpha-pinene (API) in Saxony for the year 2019, along with anthropogenic and biogenic emission data for limonene (LIM) in the same year. Emission data were obtained by averaging values across the approximated area of the entire state of Saxony (see Fig. S1). The emission data source is from the German Environment Agency (UBA) for Germany and Thürkow et al. (2024). Detailed data can be referred to Table S12.

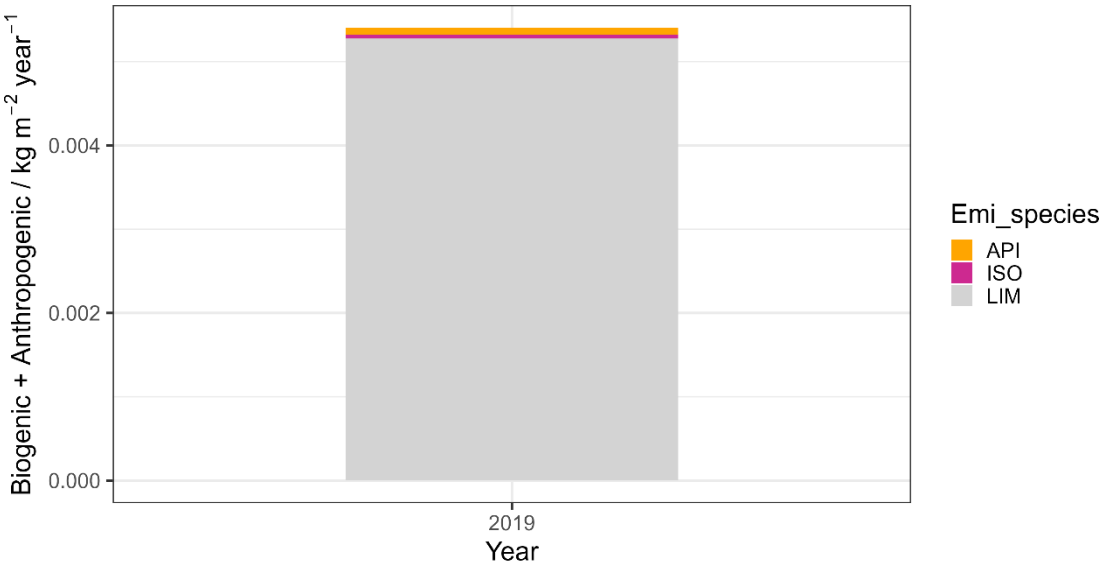

Figure S17: Biogenic emissions of isoprene (ISO) and alpha-pinene (API) in urban area for the year 2019, along with anthropogenic and biogenic emission data for limonene (LIM) in the same year. Emission data were obtained by averaging values from the selected urban area (city of Leipzig) (see Fig. S1). The emission data source is from the German Environment Agency (UBA) for Germany and Thürkow et al. (2024). Detailed data can be referred to Table S12.

Table S12. A summary of the emission data from Figs. S16 and S17.

Emission species	Emission source	Saxony	Leipzig-urban
		Emission / kg m^{-2} year^{-1}	
Alpha-pinene	Biogenic emissions	0.00098	0.00008
Isoprene	Biogenic emissions	0.00041	0.00005
Limonene	Anthropogenic and biogenic emissions	0.00073	0.00528

Table S13: Emission categories and corresponding emission sectors (Schneider et al., 2016).

See attached Excel file named *Table S13_Emission categories and corresponding emission sectors.*

Reference

Clifton, O. E., Fiore, A. M., Massman, W. J., Baublitz, C. B., Coyle, M., Emberson, L., Fares, S., Farmer, D. K., Gentine, P., and Gerosa, G.: Dry deposition of ozone over land: processes, measurement, and modeling, Reviews of Geophysics, 58, e2019RG000670, https://doi.org/10.1029/2019RG000670, 2020.

Herrmann, H., Ervens, B., Jacobi, H.-W., Wolke, R., Nowacki, P., and Zellner, R.: CAPRAM2. 3: A chemical aqueous phase radical mechanism for tropospheric chemistry, Journal of Atmospheric Chemistry, 36, 231-284, https://doi.org/10.1023/A:1006318622743, 2000.

Hoffmann, E. H., Tilgner, A., Vogelsberg, U., Wolke, R., and Herrmann, H.: Near-explicit multiphase modeling of halogen chemistry in a mixed urban and maritime coastal area, ACS Earth Space Chem., 3, 2452-2471, https://doi.org/10.1021/acsearthspacechem.9b00184, 2019.

Jaidan, N., El Amraoui, L., Attié, J.-L., Ricaud, P., and Dulac, F.: Future changes in surface ozone over the Mediterranean Basin in the framework of the Chemistry-Aerosol Mediterranean Experiment (ChArMEx), Atmospheric Chemistry and Physics, 18, 9351-9373, https://doi.org/10.5194/acp-18-9351-2018, 2018.

Pandey Deolal, S., Henne, S., Ries, L., Gilge, S., Weers, U., Steinbacher, M., Staehelin, J., and Peter, T.: Analysis of elevated springtime levels of Peroxyacetyl nitrate (PAN) at the high Alpine research sites Jungfraujoch and Zugspitze, Atmospheric Chemistry and Physics, 14, 12553-12571, https://doi.org/10.5194/acp-14-12553-2014, 2014.

Python Software Foundation: Python Language Reference, version 3.10. http://www.python.org, 2021.

Rondón, A., Johansson, C., and Granat, L.: Dry deposition of nitrogen dioxide and ozone to coniferous forests, Journal of Geophysical Research: Atmospheres, 98, 5159-5172, https://doi.org/10.1029/92JD02335, 1993.

Schneider, C., Pelzer, M., Toenges-Schuller, N., Nacken, M., and Niederau, A.: ArcGIS basierte Lösung zur detaillierten, deutschlandweiten Verteilung (Gridding) nationaler Emissionsjahreswerte auf Basis des Inventars zur Emissionsberichterstattung, Dessau. Roßlau Retrieved, 27, 2019, https://www.umweltbundesamt.de, 2016.

Stieger, B., Spindler, G., Fahlbusch, B., Müller, K., Grüner, A., Poulain, L., Thöni, L., Seitler, E., Wallasch, M., and Herrmann, H.: Measurements of PM 10 ions and trace gases with the online system MARGA at the research station Melpitz in Germany–A five-year study, Journal of Atmospheric Chemistry, 75, 33-70, https://doi.org/10.1007/s10874-017-9361-0, 2018.

Thürkow, M., Schaap, M., Kranenburg, R., Pfäfflin, F., Neunhäuserer, L., Wolke, R., Heinold, B., Stoll, J., Lupaşcu, A., and Nordmann, S.: Dynamic evaluation of modeled ozone concentrations in Germany with four chemistry transport models, Science of the Total Environment, 906, 167665, https://doi.org/10.1016/j.scitotenv.2023.167665, 2024.

Wu, Z., Wang, X., Turnipseed, A. A., Chen, F., Zhang, L., Guenther, A. B., Karl, T., Huey, L., Niyogi, D., and Xia, B.: Evaluation and improvements of two community models in simulating dry deposition velocities for peroxyacetyl nitrate (PAN) over a coniferous forest, Journal of Geophysical Research: Atmospheres, 117, D04310, https://doi.org/10.1029/2011JD016751, 2012.

Yu, S., Eder, B., Dennis, R., Chu, S. H., and Schwartz, S. E.: New unbiased symmetric metrics for evaluation of air quality models, Atmospheric Science Letters, 7, 26-34, https://doi.org/10.1002/asl.125, 2006.

Zellweger, C., Hüglin, C., Klausen, J., Steinbacher, M., Vollmer, M., and Buchmann, B.: Inter-comparison of four different carbon monoxide measurement techniques and evaluation of the long-term carbon monoxide time series of Jungfraujoch, Atmospheric Chemistry and Physics, 9, 3491-3503, https://doi.org/10.5194/acp-9-3491-2009, 2009.

Zhu, Y., Tilgner, A., Hoffmann, E. H., Herrmann, H., Kawamura, K., Yang, L., Xue, L., and Wang, W.: Multiphase MCM–CAPRAM modeling of the formation and processing of secondary aerosol constituents observed during the Mt. Tai summer campaign in 2014, Atmospheric Chemistry and Physics, 20, 6725-6747, https://doi.org/10.5194/acp-20-6725-2020, 2020.